AGU PUBLICATIONS

Journal of Geophysical Research: Space Physics

RESEARCH ARTICLE

10.1002/2014JA020138

Key Points:

- Regions 1 and 2 field-aligned current magnitudes are associated
- Dayside/nightside reconnection drives FAC magnitudes
- In general, R1 currents are stronger than R2 currents

Correspondence to:
J. C. Coxon,
jcc19@leicester.ac.uk

Citation:
Coxon, J. C., S. E. Milan, L. B. N. Clausen, B. J. Anderson, and H. Korth (2014), The magnitudes of the regions 1 and 2 Birkeland currents observed by AMPERE and their role in solar wind-magnetosphere-ionosphere coupling, *J. Geophys. Res. Space Physics*, *119*, 9804–9815, doi:10.1002/2014JA020138.

Received 5 MAY 2014
Accepted 7 NOV 2014
Accepted article online 11 NOV 2014
Published online 12 DEC 2014

The magnitudes of the regions 1 and 2 Birkeland currents observed by AMPERE and their role in solar wind-magnetosphere-ionosphere coupling

J. C. Coxon[1], S. E. Milan[1], L. B. N. Clausen[2], B. J. Anderson[3], and H. Korth[3]

[1]Department of Physics and Astronomy, University of Leicester, Leicester, UK, [2]Department of Physics, University of Oslo Oslo, Norway, [3]Johns Hopkins University Applied Physics Laboratory, Laurel, Maryland, USA

Abstract In this paper we present the first large-scale statistical study of the influence of magnetic reconnection on the magnitude of the regions 1 and 2 Birkeland field-aligned currents (FACs). While previous studies have employed single spacecraft measurements to construct a statistical picture of the location and density of the Birkeland currents, it has hitherto been difficult to compare in situ measurements of the solar wind with instantaneous global field-aligned current measurements. To that end, we utilize the Active Magnetosphere Planetary Electrodynamics Response Experiment (AMPERE), which yields field-aligned current density in both hemispheres at a cadence of 10 min. We quantify the amount of current flowing in the regions 1 (R1) and 2 (R2) FACs, and we compare these with the dayside reconnection rate Φ_D deduced from interplanetary parameters from the OMNI data set and with the *AL* index to examine whether magnetic reconnection is responsible for driving currents in the coupled magnetosphere-ionosphere system. We find that current magnitudes are strongly correlated with both Φ_D and *AL* index. We also find that R1 currents tend to be higher than R2 currents during periods of magnetic reconnection, suggesting leakage of current across the polar cap or an association with the substorm current wedge.

1. Introduction

The existence of field-aligned currents were first proposed at the start of the twentieth century [*Birkeland*, 1908, 1913], and it is now known that the Birkeland field-aligned current system is responsible for electrodynamically linking the magnetopause, the inner magnetosphere, and the ionosphere. The magnetic perturbations associated with this current system were first detected in space by the polar orbiting satellite 1962 38C [*Zmuda et al.*, 1966]. The large-scale morphology of the currents was first deduced using Triad satellite observations [*Iijima and Potemra*, 1976a, 1976b, 1978].

Broadly speaking, the current system forms two concentric rings above the auroral ionosphere: the poleward (region 1) ring and the equatorward (region 2) ring. *Iijima and Potemra* [1978] observed that the two regions appear to be driven by different parts of the system: the region 1 (R1) currents connect the ionosphere to currents in the magnetopause (also known as the Chapman-Ferraro currents) and the magnetotail, and the region 2 (R2) currents connect to the partial ring current in the inner magnetosphere [e.g., *Cowley*, 2000, *Clausen et al.*, 2012]. Region 1 currents flow upward in the dusk sector and downward in the dawn sector, and region 2 currents are of opposite polarity. R1 currents are colocated with the flow shear between sunward and antisunward plasma flow across the polar cap associated with twin-cell ionospheric convection [*Dungey*, 1961; *Cowley and Lockwood*, 1992; *Cowley*, 2000]. The regions 1 and 2 currents close through the ionosphere via horizontal Pedersen currents. This system is sketched schematically in Figure 1. The arrow across the polar cap is smaller because the Pedersen currents that close R1 through R1 across the polar cap are smaller than those flowing in the auroral zone. In the rest of this paper, upward currents will be considered positive while negative values represent downward currents.

It is noted in *Iijima and Potemra* [1978] that the dawn and dusk current systems overlap in the region of magnetic local time (MLT) where $20 \leq \text{MLT} \leq 24$, in what is known as the Harang discontinuity region. There is also a third system that appears poleward of the region 1 currents on the dayside of the planet and is associated with the dayside cusp (sometimes denoted region 0). Also, *Iijima and Potemra* [1976b] noted that the region 1 currents appear to dominate on the dayside whereas the region 2 currents appear to dominate on the nightside.

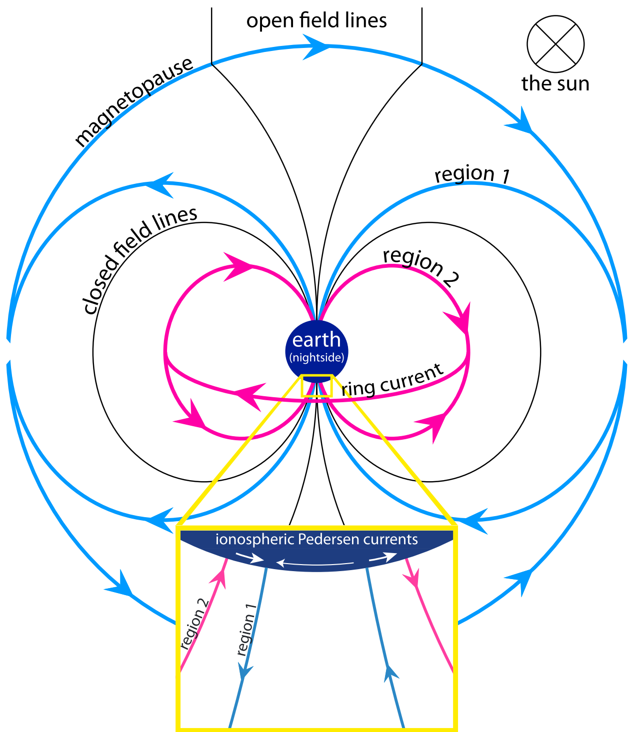

Figure 1. A diagram drawn as if Earth was eclipsing the Sun. It shows the region 1, region 2, Pedersen, magnetopause (Chapman-Ferraro), and ring currents as well as illustrating the location of open and closed terrestrial magnetic field lines. The arrow showing Pedersen current flow across the polar cap is smaller than the arrows for the auroral zone to indicate the relative strength of the Pedersen currents (not to scale). It can be seen from this image how the region 1 current sheet corresponds to the open/closed field line boundary, or OCB.

The Birkeland currents are associated with the polar ionosphere convection pattern, which is also associated with the Dungey cycle [*Dungey*, 1961], driven by magnetic reconnection at the magnetopause and in the magnetotail [*Cowley and Lockwood*, 1992]. *Clausen et al.* [2012, 2013a, 2013b] have shown that the Birkeland currents change in latitude in a manner consistent with the expanding/contracting polar cap (ECPC) paradigm of the excitation of the Dungey cycle [*Milan et al.*, 2003, 2007; *Milan*, 2013]. It is the purpose of this paper to characterize the magnitudes of the currents and relate them to this picture of the solar wind-magnetosphere-ionosphere coupled system.

The Dungey cycle is the circulation of Earth's magnetic field and plasma in the magnetosphere caused by magnetic reconnection between the Interplanetary Magnetic Field (IMF) frozen into the outflowing solar wind and the terrestrial dipole [*Dungey*, 1961]. This creates "open magnetic flux" interconnecting the interplanetary medium to the polar regions. Subsequently, reconnection in the tail closes this open magnetic flux, and it returns to the dayside to complete the cycle. It is this opening and closing of flux that drives magnetospheric convection and a sympathetic circulation of plasma in the ionosphere. As dayside reconnection occurs, the amount of open magnetic flux inside Earth's magnetosphere increases. Nightside reconnection reduces the amount of open magnetic flux in the same way. The amount of open magnetic flux in the magnetosphere governs the location of the boundary between the open and closed flux in the ionosphere, enclosing the area known as the polar cap—when there is more open magnetic flux, the boundary is farther from the pole, and therefore the size of the polar cap is increased.

Stresses are transmitted around the system by current systems, and the R1/R2 currents are an integral component. The region 1 Birkeland currents are believed to flow, in part, within the boundary between the open and closed flux, also called the OCB [*Clausen et al.*, 2012]. Therefore, an accurate calculation of their location can be used as a proxy for the size of the polar cap and this means that any such measurement can also be used to determine the ratio of open to closed magnetic flux in the Earth's magnetosphere. By taking the time derivative of the location of the current ovals, the net magnetic reconnection rate can be calculated. In this paper we characterize the magnitudes of the R1 and R2 currents using the Active Magnetosphere Planetary Electrodynamics Response Experiment (AMPERE) technique outlined in section 2, which are in turn related to the strength of the convection pattern driven by the dayside and nightside reconnection rates and the conductance of the ionosphere.

2. The AMPERE Data Set

The Active Magnetosphere and Planetary Electrodynamics Experiment (AMPERE) was conceived to investigate the Birkeland currents using magnetometer data from the Iridium® telecommunications satellite network [*Anderson et al.*, 2000]. The Iridium® network comprises 66 active spacecraft that orbit the Earth in six polar orbital planes at an altitude of 780 km. Eleven spacecraft are found in each plane, and each is in a

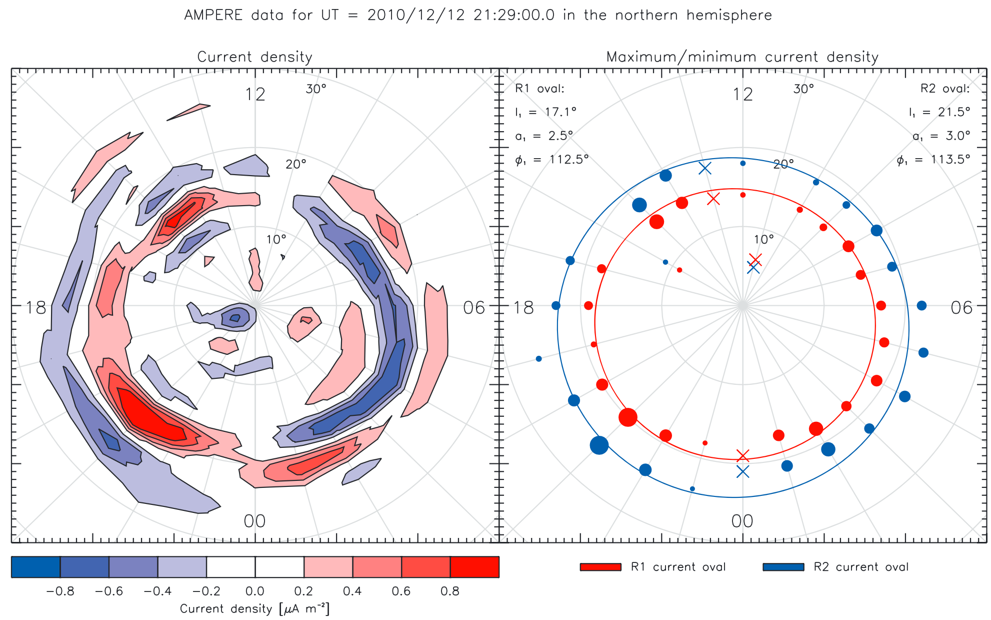

Figure 2. (left) Current density at UT = 12 December 2010 21:29:00 in the Northern Hemisphere. (right) Current locations, plotted as circles, obtained using equation (1) over all MLT, with overlaid fitted current ovals as red (R1) and blue (R2) lines produced by equation (2). Radial lines indicate meridians of MLT, with 12 MLT at the top of the diagram. Concentric circles indicate geomagnetic latitude in steps of 10°. Circles' size is proportional to the value of a_0 in the eventual fit. Crosses denote meridians for which no good fit was found. (Note that red and blue change in meaning between the two diagrams.)

circular, polar orbit that takes 104 min to complete. These six orbital planes provide measurements along 12 MLT meridians (two values of MLT per orbital plane).

Satellites in the constellation are fitted with a triaxial magnetometer for the purposes of determining the satellite's attitude and keeping the spacecraft oriented toward the nadir. Large perpendicular magnetic perturbations $\Delta\vec{b}$ from the main field $\vec{B}_0$ indicate the presence of FACs. The Birkeland current sheets largely extend from east to west, so the perturbations will be perpendicular to any polar orbit [*Waters et al.*, 2001]. *Anderson et al.* [2000] used the cross track component of the magnetic perturbation to deduce the field-aligned current magnitude and concluded that the Iridium® constellation data were useful for characterization of large-scale FACs in both hemispheres on time scales of several hours or less.

The AMPERE data set used in this study contains maps of Birkeland currents in the Northern and Southern Hemispheres, made at 10 min cadence for the period from January 2010 to December 2012.

Figure 2 (left) shows a contour map of the current density observed by AMPERE at 21:29 on 12 December 2010. Upward currents are shown in red (positive values) and downward currents in blue (negative). As discussed in section 1, in general, there are two rings of current: the inner region 1 current and the outer region 2 current. However, there are exceptions to the rule; for instance, at the 14 MLT meridian where two downward regions clearly flank a single upward region.

In this study we are interested in the large-scale morphology of the R1/R2 system and wish to suppress small-scale, rapidly varying features. To characterize the location and strength of the Birkeland current ovals, we use the fitting method described by *Clausen et al.* [2012]. This method determines the latitudes of the R1 and R2 currents along each meridian separately, before combining this information to determine the radii of the R1 and R2 current ovals (Figure 2, right).

Figure 3 presents a plot of current density j against latitude l for MLT = 18 in Figure 2 (left), demonstrating the bipolar signature expected for adjacent upward and downward current sheets. *Clausen et al.* [2012] proposed a sinusoid with a Gaussian envelope which can be fitted to the bipolar deflection to identify the R1

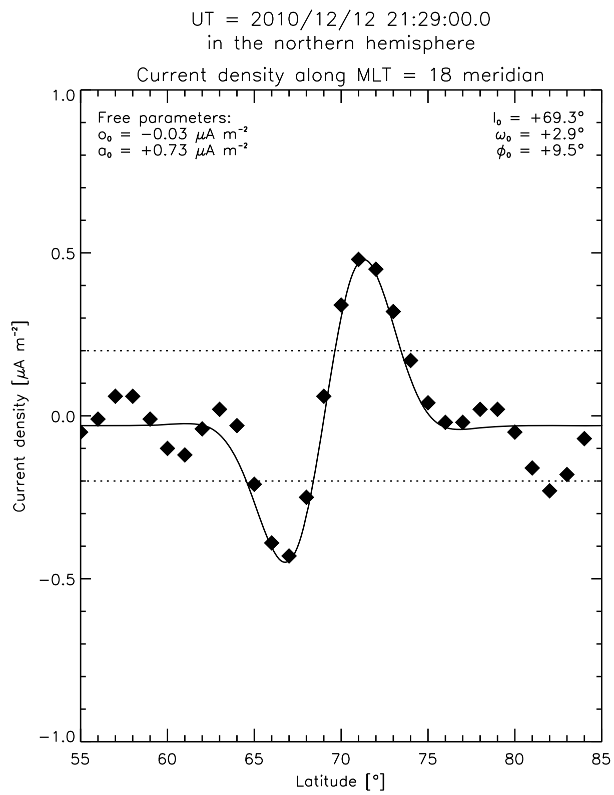

Figure 3. Current density plotted against latitude along the dusk meridian as diamonds. The solid black line is the fit obtained by equation (1), whereas the dotted lines indicate the lowest current density plotted in Figure 2.

and R2 current systems. They also concluded that it was sensible to neglect small-scale current signatures below 0.2 μA m^{-2}, shown by a broken line in Figure 3. Their equation is given by

$$j_{\mathrm{fit}}(l) = o_0 + a_0 \exp\left(-\frac{(l-l_0)^2}{2\omega_0^2}\right) \sin\left(2\pi \frac{l-l_0}{2\sqrt{8\ \ln\ 2}\omega_0} + \phi_0\right) \quad (1)$$

where o_0 is the zero offset, a_0 is the amplitude, and l_0 is the location of the center of the function. The full width at half maximum (FWHM) of the Gaussian is given by $\sqrt{8\ \ln\ 2}\omega_0$, and the wavelength of the sinusoid was chosen to be twice the FWHM. The parameter ϕ_0 is the phase shift of the sinusoid, such that the sinusoid crosses the line of $J = o_0$ at $l = l_0 - 2\sqrt{8\ \ln\ 2}\omega_0\phi_0/2\pi$. An illustration of these parameters can be found in Figure 3 of *Clausen et al.* [2012].

An algorithm was created to automatically fit this equation to AMPERE data using a method outlined by *Milan et al.* [2012] in which a program starts with reasonable guesses for each parameter and iterates to find the best values of each. A fit line found by this algorithm is superimposed on Figure 3. We do not attempt to calculate a fit where the maximum current density detected is less than 0.2 μA m^{-2}. We reject fits on the dawnside where an upward current is detected poleward of a downward current and vice versa on the duskside, since these are inconsistent with the R1/R2 current system. We also reject fits where $\omega_0 < 1.0$, $|\phi_0| > 50°$, or $l_0 > 85°$.

Figure 2 (right) shows the result of fitting to each of the meridians, where the dots indicate the locations of the upward and downward current peaks and the size of the dots are an indication of current density. It should be noted that red and blue are used to indicate upward and downward currents in Figure 2 (left) but are used to indicate R1 and R2 currents in Figure 2 (right). These fits can be used in turn to identify the size of the current rings. *Clausen et al.* [2012] gave an equation that can be used to get a fit to these points:

$$f(m) = l_1 + a_1 \cos\left(\frac{2\pi m}{24} + \phi_1\right) \quad (2)$$

where m is the MLT, l_1 is the mean latitude of the oval, a_1 is the amplitude of the deviation from the mean latitude and ϕ_1 is the oval's phase offset. We fit this equation to the data using the same method as for equation (1), and the result can be seen in the fit lines plotted in Figure 2 (right).

We calculate the overall current magnitude flowing in each of the rings by integrating under the fitted curve of Figure 3 between the midpoint and the poleward edge (R1)/the equatorward edge (R2). The midpoint is given by $x = l_0 - 2\sqrt{8\ln 2}\omega_0\phi_0/2\pi$, and the equatorward and poleward edges are located at 0° and 60° colatitude (since the contribution of any colatitude at which $y = o_0$ is zero). We multiply by the area in m^2 described by a 0.1° by 1 MLT segment: For the case of Figure 3, the R1 and R2 currents integrated from 17:30 to 18:30 MLT have magnitudes of 140 and −118 kA, respectively; summing across all the meridians seen in Figure 2 gives values of R1 current flowing J_1 = 3.4 MA and R2 current flowing J_2 = 2.7 MA, yielding a ratio $J_1/J_2 \sim 1.3$. It should be noted that we normalize the current magnitudes in the dawn and dusk sectors by

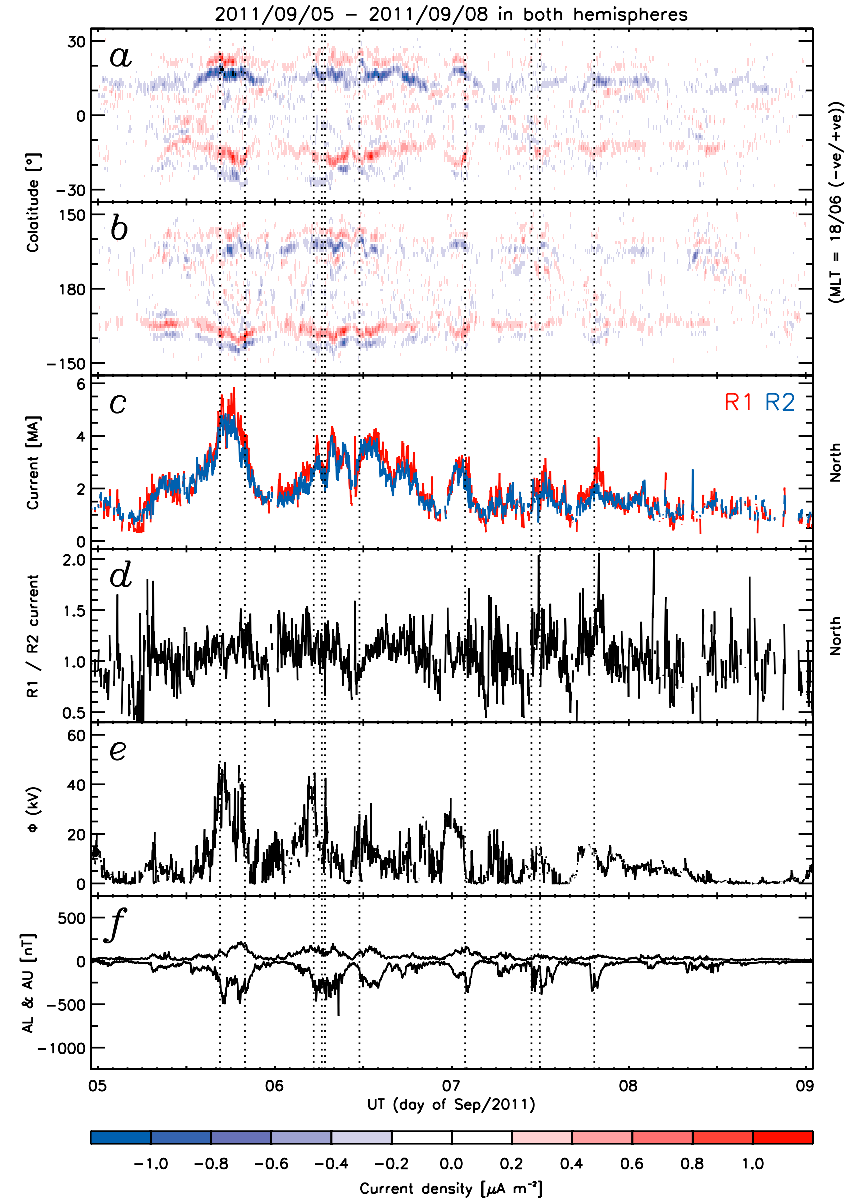

Figure 4. Diagram showing the 4 days beginning at UT = 2010-02-01 00:00:00. From top to bottom: Keograms showing the dawn-dusk meridian for (a) the Northern Hemisphere and (b) the Southern Hemisphere; (c) the R1 current magnitude I_{R1} (red) and R2 current magnitude I_{R2} (blue) for the Northern Hemisphere; (d) I_{R1}/I_{R2} in the Northern Hemisphere; (e) the dayside reconnection rate Φ_D; f) the *AL* and *AU* indices. Vertical dashed lines represent the locations of substorms from the SuperMAG substorm list [*Newell and Gjerloev*, 2011a, 2011b].

dividing by the number of fitted meridians and multiplying by 12 in both before summing the two sectors, so the numbers presented may be slightly overestimated.

3. Currents Driven by Solar Wind-Magnetosphere-Ionosphere Coupling

3.1. Four Day Example of Reconnection Driving the Birkeland Currents

As outlined in section 1, the magnitudes of the Birkeland currents should be driven by magnetic reconnection on both the dayside and the nightside of Earth's magnetosphere. As a result, it is desirable to examine the reaction of the Birkeland currents to both dayside and nightside reconnection rate. Previously, papers

10.1002/2014JA020138

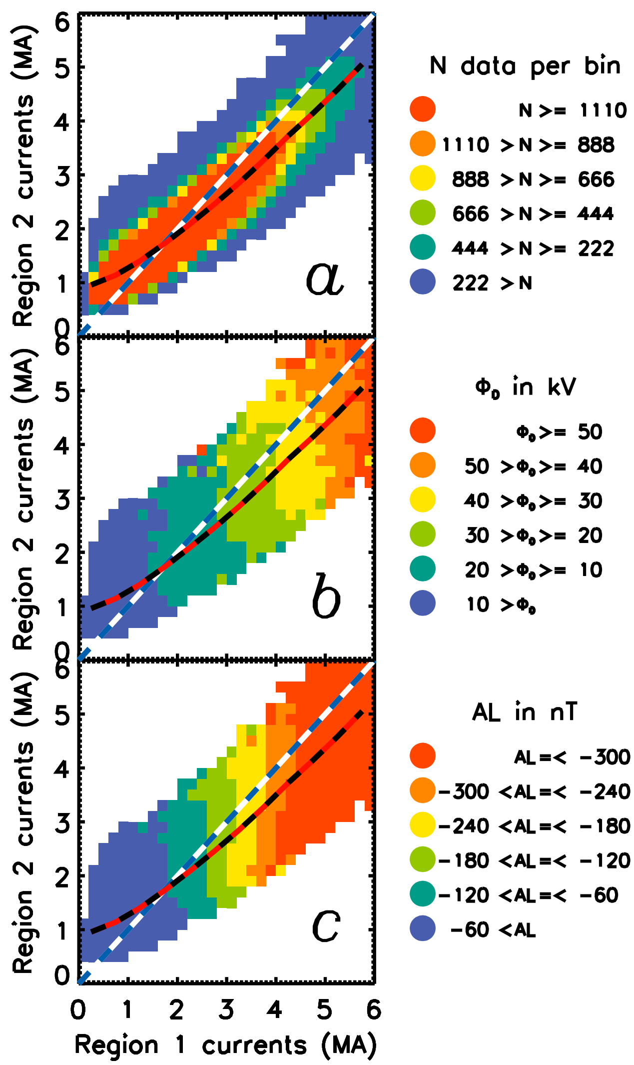

Figure 5. A graph showing J_1 plotted on *x* and J_2 plotted on *y*, color coded by (a) number of data per bin, (b) dayside reconnection rate Φ_D in kV, and (c) *AL* index in nT. Where there are fewer than 10 data contributing to a bin, that bin is left white. The color code for each panel is to the right of the panel.

have modeled the dayside reconnection rate Φ_D [e.g., *Gonzalez and Mozer*, 1974; *Milan et al.*, 2012, and references therein]. We use the expression given by *Milan et al.* [2012]:

$$\Phi_D = L_{\text{eff}}(V_X)V_X B_{YZ} \sin^{\frac{9}{2}}\left(\frac{\theta}{2}\right) \quad (3)$$

In the above equation, $L_{\text{eff}}(V_X)$ is an effective length scale, given by

$$L_{\text{eff}}(V_X) = 3.8\, R_E \left(\frac{V_X}{4 \times 10^5 \text{ m s}^{-1}}\right)^{\frac{1}{3}} \quad (4)$$

and B_{YZ} is the transverse component of the IMF, given by

$$B_{YZ}^2 = B_Y^2 + B_Z^2. \quad (5)$$

V_X is the solar wind speed, θ is the clock angle between the IMF vector projected into the GSM *Y-Z* plane and *Z* axis, and R_E is the radius of Earth.

Figures 4a and 4b depict the Birkeland current density as a cut along the dawn-dusk meridian as observed by AMPERE in the Northern and Southern Hemispheres respectively for a 4 day period in September 2010. This format shows the magnitudes of the currents as well as the spatial distribution, especially the variations in latitude at which currents are observed. Figure 4c presents the magnitude of R1, R2, J_1, and J_2, calculated as before. Figure 4d shows the ratio J_1/J_2. Figure 4e shows Φ_D as calculated by equation (3), and Figure 4f shows the *AL* and *AU* indices.

Figures 4a–4c show that the current density varies significantly with time, including periods of quiescence (before 06:00 on 5 September and after 04:00 on 8 September) and periods of stronger currents seen throughout the rest of the interval. The current densities vary up to 1.2 μA m^{-2} both downward (blue) and upward (red), with higher densities seen in the Southern Hemisphere (the summer hemisphere). Stronger currents occur during periods of strong dayside reconnection and weaker currents occur when dayside reconnection wanes (Figure 4e). The Pearson correlation coefficient $r = 0.60$ for Φ_D and J_1, and $r = 0.61$ with J_2, demonstrating a correlation during this period. The *AL* and *AU* indices shown in Figure 4f also have quiet periods at the start and end of the interval, with very little activity before 07:00 on day 1 and very little activity after 04:00 on day 4.

The current magnitudes in Figure 4c vary between 1 and 4 MA for most of the intervals, with dips to 0.5 MA and peaks of 6 MA also observed. However, there are also periods in which the current densities are too low for the fitting technique to work. The first period falls within the first low current density interval, occurring between 00:00 and 04:00 on 5 September. The next periods occur between periods of stronger current density: at 00:00 and 23:00 on 6 September and 10:00 and 14:00 on 7 September. The final period is after 04:00 on 8 September, in the final quiescent period.

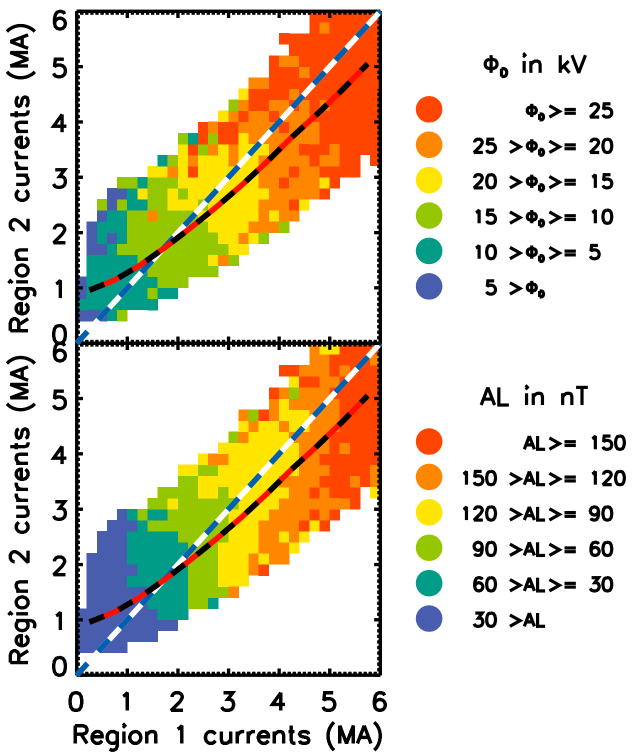

Figure 6. A graph showing J_1 plotted on *x* and J_2 plotted on *y*, color coded by the standard deviation of (top) dayside reconnection rate Φ_D in kV and (bottom) *AL* index in nT. Where there are fewer than 10 data contributing to a bin, that bin is left white. The color code for each panel is to the right of the panel: the colors are half the values of Figure 5.

The current ovals are located between colatitudes of 10° and 30°. These vary in latitude, several excursions occurring in both hemispheres simultaneously, associated with expansions and contractions of the polar cap [*Clausen et al.*, 2013a]. Substorm onsets are identified by characteristic negative bays in *AL*, marked by vertical dashed lines. We see that each substorm onset is preceded by a movement of the currents to lower latitude (substorm growth phase) and are followed by contractions to a higher latitude (substorm expansion phase). Substorms are, in general, associated with increases in current magnitude: the Pearson coefficient $r = -0.55$ between *AL* index and J_1 and between *AL* and J_2. These are slightly lower correlations than those seen with Φ_D.

In order to assess the effect of both Φ_D and *AL* index on the Birkeland current magnitudes, we calculate the multiple correlation coefficient [*Neter et al.*, 1988]. This has been calculated using the method outlined by *Cohen et al.* [2003, equation (3.3.1)], given by

$$R = \left(\frac{r_{Y1}^2 + r_{Y2}^2 - 2r_{Y1}r_{Y2}r_{12}}{1 - r_{12}^2} \right)^{0.5} \quad (6)$$

where r_{12} is the Pearson correlation between the two independent variables (*AL* index and Φ_D in this case), and r_{Y1} and r_{Y2} are the two Pearson correlations between the dependent variable (*J*) and the two independent variables. We find that the multiple correlation coefficient for J_1 is 0.89 and for J_2 is 0.87, both strong correlations.

3.2. Current Magnitude Variations With Magnetic Reconnection on the Dayside and Nightside

Now we have examined the temporal variation of the current systems, we turn to the statistical relationship between R1 and R2 current magnitude and dayside and nightside driving by employing 3 years of AMPERE data (2010–2012). The magnitudes of the region 1 Birkeland currents have been plotted against the magnitudes of the region 2 currents, shown in Figure 5a as an occurrence frequency diagram with bins of 0.2 MA.

The magnitudes of the Birkeland currents are strongly positively correlated, but the figure is asymmetrical about the white and blue dashed line which shows the line of equality. At low current magnitudes, J_1 and J_2 are roughly equal, although J_1 begins to dominate over J_2 above 1.5 MA and J_2 seemingly dominates at very low magnitudes. At higher R1 currents, the ratio J_1/J_2 increases on average to about 1.15, as indicated by the red and black dashed line, which is a plot of the mean of J_2 in a series of bins of J_1, which are 0.25 MA wide, effectively giving the ratio between the two.

The color coding in Figure 5a shows the number of data in each of the plotted bins. This shows that the majority of the AMPERE data set is made up of currents in both regions between approximately 0.4 MA and 5 MA. Figure 5b depicts the currents' magnitudes color coded by the mean of Φ_D in a given pixel,

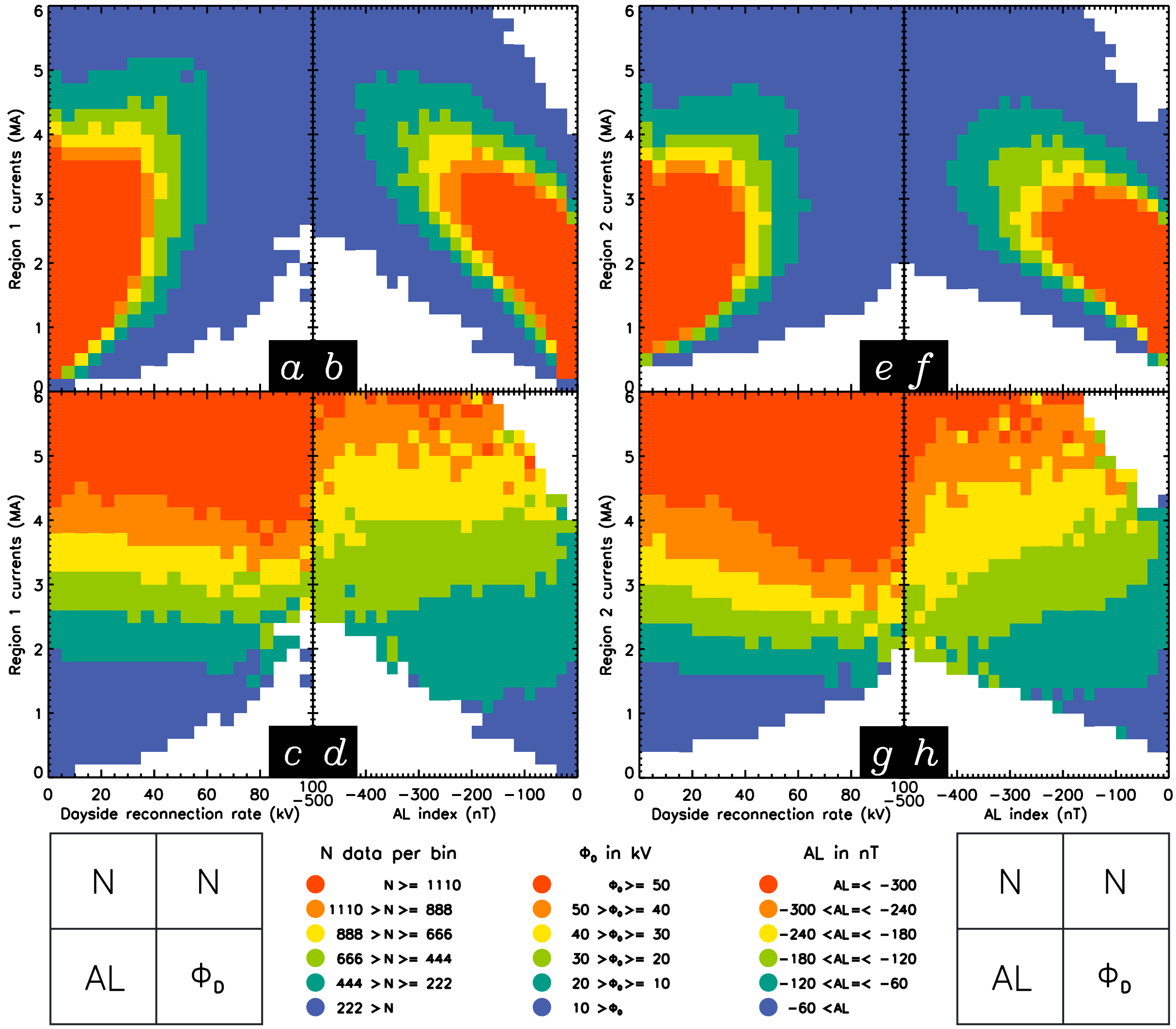

Figure 7. (a–d) J_1 and (e–h) J_2 plotted against Φ_D (Figures 7a, 7c, 7e, and 7g) and AL index (Figures 7b, 7d, 7f, and 7h). These are then color coded by number of data per bin (Figures 7a, 7b, 7e, and 7f), by *AL* index in nT (Figures 7c and 7g) or by Φ_D in kV (Figures 7d and 7h). Where there are fewer than 10 data contributing to a bin, that bin is left white. The color codes are given underneath (and are the same as those for Figure 5); the grids on either side describe the variable by which each panel is color coded.

whereas in Figure 5c they appear color coded by the mean of *AL* index, since it has been shown that westward electrojet current is approximately proportional to the nightside reconnection rate [*Holzer et al.*, 1986]. It is immediately obvious that the two are very similar; both dayside and nightside reconnection rates are expected to drive Birkeland current magnitude.

Higher currents are clearly correlated to faster reconnection. The Pearson coefficient $r = 0.64$ for Φ_D and J_1 and $r = 0.63$ in the case of J_2, showing that R1 currents are slightly more correlated. Correlating the two with *AL* index, we find for J_1, $r = -0.83$, and for J_2, $r = -0.78$, showing that R1 currents are again more correlated. The coefficient of multiple correlation of J_1 with Φ_D and *AL* index is found to be 0.85, and the coefficient of multiple correlation of J_2 with both drivers is 0.81. The standard deviations of the values from Figure 5 are shown in Figure 6.

3.3. Solar Wind Driving of the Birkeland Currents Combined With Dayside and Nightside Reconnection Rates

Figure 7 shows the Birkeland current magnitudes plotted against dayside reconnection rate Φ_D (Figures 7a, 7c, 7e, and 7g) and against the *AL* index (Figures 7b, 7d, 7f, and 7h). Figures 7a, 7b, 7e, and 7f show this

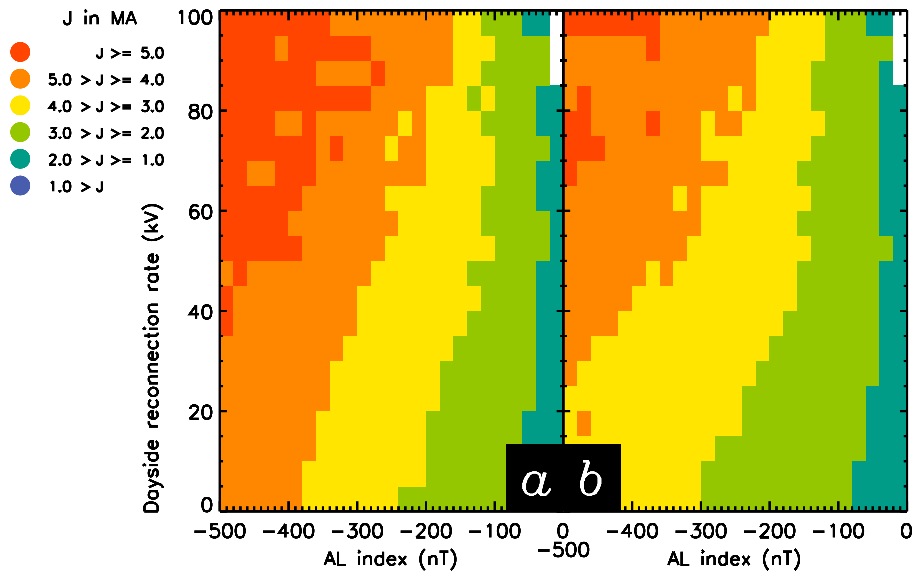

Figure 8. Panels showing *AL* index plotted against Φ_D, color coded by (a) J_1 and (b) J_2. Where there are fewer than 10 data contributing to a bin, that bin is left white. The color code is depicted on the left and is the same for both J_1 and J_2.

relationship color coded by the number of data per bin N (the color coding is the same between Figures 5 and 7 for every variable). It can be seen that the majority of the points lie where $I < 5$ MA and either $\Phi_D < 50$ kV or $AL > -300$ nT, with small amounts of data elsewhere in the parameter space. The correlation between current magnitude and dayside reconnection rate can be seen in the main population (those bins not colored blue), which clearly shows that higher current magnitudes are observed for higher values for Φ_D. A similar correlation can be seen for *AL* index.

First, we focus on the relationship between the Birkeland currents and the dayside reconnection rate. Figures 7a and 7e highlight that R1 is generally slightly more strongly correlated with Φ_D than R2 is. Figure 7c shows the same parameter space as in Figure 7a but this time color coded by *AL* index. In R1, a given magnitude is strongly correlated with a specific value of *AL* index, as visible in the almost horizontal striations in the color coding by *AL*, with magnitudes of below 2 MA correlated with an *AL* index of above −60 nT and magnitudes above 4 MA correlated with an *AL* index of below −300 nT. In R2, as shown by Figure 7g, a given magnitude is driven by either a high dayside reconnection rate and high *AL* index, as seen by 3 MA currents occurring at $\Phi_D \simeq 90$ kV and an *AL* index of approximately −200 nT, or by a low dayside reconnection rate and slightly lower *AL* index, as seen by 3 MA currents occurring at $\Phi_D < 20$ kV and $AL \simeq -80$ nT.

Turning now to the *AL* index, we can see from Figures 7b and 7f that R1 current is more correlated with *AL* index than R2 current is. Figure 7d is color coded by Φ_D, which shows striations in R1 currents similar to those in Figure 5. R1 currents of around 2 MA are driven by $\Phi_D \simeq 20$ kV whereas R1 currents of around 4 MA are driven by $\Phi_D \simeq 40$ kV. Figure 7h shows that R2 currents of 3 MA can be driven by high *AL* index and high dayside reconnection (∼ 40 kV, ∼ −400 nT) or by low dayside reconnection and a lower *AL* index (∼ 20 kV, ∼ −100 nT).

Finally, we present Figure 8, which shows the parameter space of *AL* index versus dayside reconnection rate color coded by R1 and R2 Birkeland current magnitude (Figures 8 and 8b, respectively). This clearly indicates that for a given combination of Φ_D and *AL* index, the R1 currents tend to be of higher magnitudes. The diagram also demonstrates that R1, again, can be driven to higher magnitudes by purely the *AL* index, reinforcing the observed disparity in correlation between the two current systems and *AL*. At an *AL* index of −275 nT with no dayside reconnection, for example, 3.0 MA ≤ R1 < 4.0 MA, whereas 3.0 MA ≤ R2 < 2.0 MA.

4. Discussion

We have used observations from the AMPERE data set to estimate the current magnitudes flowing in the regions 1 and 2 Birkeland current system. We have demonstrated that these currents are dependent on the dayside reconnection rate quantified by Φ_D, and nightside reconnection, for which we use the *AL* auroral geomagnetic index as a proxy. We now discuss these findings in more detail.

Comparing the magnitudes of the R1 and R2 currents we find that the currents are approximately equal at a magnitude of $\sim$ 1.5 MA (Figure 5a). R1 currents begin to dominate above this point and the currents are, for values greater than $\sim$ 1.5 MA, in the ratio $J_1/J_2 \simeq 1.15$ (which is slightly lower than those in the interval shown in Figures 2 and 3). This is explained as R2 currents must close through ionospheric Pedersen currents to the R1 currents, whereas R1 currents can additionally close via Pedersen currents across the polar cap through R1 currents of the opposite polarity (see Figure 1). It is also possible that the R1 currents can flow across the high-conductance auroral bulge. At times of low current magnitude and therefore low geomagnetic activity, the polar cap is likely to be of lower conductance, impeding the flow of Pedersen currents such that the R1 current system must close through the R2 current system, explaining the lack of R1 dominance at lower magnitudes. We also observe times at which $J_1/J_2 < 1$, indicating more current flowing in the R2 current system (this can be seen in Figure 5 and also in Figure 4, particularly after substorms vi and vii). The R2 domination is observed during periods of low reconnection rate for which we have fewer data, possibly indicating this effect is not well constrained. However, this may also indicate a relationship to the region 0 current system during periods of northward IMF. More work is required to assess the behavior of FACs during such times.

During the 4 day period presented in Figure 4, we have identified 11 substorms from their characteristic negative perturbations in the *AL* index. These substorms tend to be preceded by periods of elevated dayside reconnection Φ_D. As indicated by the measured correlation, the current systems intensify at these times and the current ovals move to lower latitudes as open magnetic flux accumulates in the magnetosphere [*Milan et al.*, 2003, 2007, 2012; *Clausen et al.*, 2012]. At the time of substorm onset the current systems retreat to higher latitudes and the currents reintensify. At some points in the period presented in Figure 4, similar current magnitudes are observed at times of somewhat different levels in Φ_D and *AL* index. This indicates that although the reconnection rate plays an important role in driving these currents, as evidenced by the strong multiple correlation coefficients, other factors (such as ionospheric conductivity) may also influence the strength of the currents flowing: this is an area of further research. During the 4 day period the J_1/J_2 ratio appears to increase such that the R1 current is stronger than R2: it is probable that this is caused by a divergence of cross-tail current through the substorm current wedge [*Clausen et al.*, 2013a, 2013b], but more work is needed to better quantify the temporal reaction of currents to substorms.

Further study of current changes through substorms, combined with observations of the convection pattern, and models which link these two phenomena [*Milan*, 2013] will play a crucial role in understanding solar wind-magnetosphere-ionosphere coupling. To this end we have studied statistically the relation of the reconnection rate to the current magnitudes (Figures 5b and 5c). The reconnection rate is observed to be driving R1 current magnitude, as the highest values of Φ_D and *AL* index are well correlated with the strongest current magnitudes. This can also be seen in the temporal presentation of the data (Figure 4): the low reconnection rates seen at the start and end of the interval appear to be driving low current densities and low current magnitudes seen in Figures 4a, 4b, and 4c. When Φ_D and *AL* index decrease after substorms vi and vii, the current density and magnitude respond by diminishing.

Previous studies have demonstrated that the ionospheric convection patterns observed in the ionosphere are driven by the direction of B_z being either north or south, with southward IMF driving a twin-cell convection pattern [*Lockwood*, 1991; *Cowley and Lockwood*, 1992] and northward IMF driving a more complex pattern [*Imber et al.*, 2006]. The location of R1 and R2 field-aligned currents is related to the structure of the ionospheric convection pattern. Our observations of higher Birkeland current magnitudes during periods of faster dayside reconnection imply that during periods of stronger ionospheric convection the Birkeland currents are enhanced, since dayside reconnection also drives ionospheric convection, and this is in agreement with previous work [*Cowley*, 2000; *Milan*, 2013; *Juusola et al.*, 2014].

Gjerloev et al. [2011] suggest that current amplitudes on the dayside are not driven by B_z. Because we expect B_z to drive Φ_D and therefore indirectly drive *J*, we decided to look at the correlation between B_z and *J*, and found that for J_1, $r = -0.46$ and, for J_2, $r = -0.43$. This is not a strong correlation, indicating that Φ_D is clearly better correlated to the current magnitudes. However, previous studies have indicated observations of stronger currents on the dayside and on the nightside during periods of southward IMF [*Rostoker et al.*, 1982; *Papitashvili*, 2002; *He et al.*, 2012; *Juusola et al.*, 2014] and case studies performed using AMPERE also support this observation [*Anderson et al.*, 2014]. As such, we interpret the observed moderate correlation as evidence for the role of B_z in current driving.

Rostoker et al. [1982] observed that, in addition to southward IMF, stronger field-aligned currents were driven by northward turnings in the IMF associated with substorms. There is some controversy on the exact mechanism by which a substorm is triggered, but our results suggest that current magnitude is enhanced alongside the *AL* index, which is associated with substorm onset and nightside reconnection. In this case we interpret the results of *Rostoker et al.* [1982] as an indication that it is nightside reconnection, rather than northward IMF, that strengthens the current.

Figures 5b and 5c depict a strong correlation between Φ_D and *AL* index with R1 currents but imply that R1 is more strongly driven than R2. We look at this relationship more closely with the aid of Figure 7. The correlations between Φ_D and J show only a 0.01 difference between R1 and R2, but R1 currents are more strongly correlated with *AL* index than R2 and *AL*, suggesting that any observed disparity in the magnitude of the two systems is more driven by periods of high *AL* index and high nightside reconnection rate.

Examining Figure 8 to further examine the reaction of currents to *AL* index, we see that R1 current is stronger at a given combination of Φ_D and *AL* index than R2, and that this effect is most pronounced during periods of low Φ_D. This further indicates that more R1 current closes through R1 when nightside reconnection dominates, which requires a greater amount of current flow across the noon-midnight meridian. Since the *AL* index is a signature of the westward substorm electrojet, we infer that this increased current flow is made possible by the substorm electrojet across the noon-midnight meridian, and that this accounts for most of the observed R1-to-R1 current closure, explaining why *AL* is better correlated to J_1/J_2 than Φ_D is.

These results suggest that reconnection plays a dominant role in exciting the currents that transfer stress to the ionosphere to produce the ionospheric convection pattern, which is known to be excited during substorm growth phase and onset [*Grocott et al.*, 2009]. It also suggests that tail dynamics and their electrical connection to the ionosphere can be monitored with this technique.

5. Conclusions

The work presented here gives an overview of the Birkeland currents on large scales in the AMPERE data set and also their reaction to the solar wind, interplanetary magnetic field, and dayside and nightside reconnection rates. It has been shown that R1 tends to be stronger than R2 at current magnitudes above ~ 1.5 MA, with the peak of the ratio between R1 and R2 being ~ 1.15 at ~ 4 MA.

The results presented in this paper can be interpreted in the context of R1 current being driven by ionospheric flows, which are ultimately driven by reconnection on the dayside and the nightside. While R2 is also well ordered by comparison to these drivers, that current system is perhaps somewhat more complex, with R2 currents weaker than R1 by *AL* index during slow dayside reconnection rates. We infer that this is a signature of the westward electrojet allowing R1 currents to close across the polar cap and through the region 1 system on the other side.

Both dayside and nightside reconnection are key to driving the Birkeland currents, with both appearing to play a vital role in strong current magnitudes. This makes sense in the context of an R1 current that maps to the magnetopause and the magnetotail, and an R2 current that maps to the partial ring current on the nightside of the Earth.

Acknowledgments
J.C.C. was supported by a Science and Technology Funding Council (STFC) studentship. S.E.M. was supported on STFC grants ST/H002480/1 and ST/K001000/1. For the Iridium-derived AMPERE data (http://ampere.jhuapl.edu/), we acknowledge the AMPERE Science Center. For the OMNI data (http://omniweb.gsfc.nasa.gov/), we acknowledge use of NASA/GSFC's Space Physics Data Facility's CDAweb service. We would like to thank the reviewers for their useful feedback.

Larry Kepko thanks Gareth Chisham and another reviewer for their assistance in evaluating this paper.

References

Anderson, B. J., K. Takahashi, and B. A. Toth (2000), Sensing global Birkeland currents with Iridium® engineering magnetometer data, *Geophys. Res. Lett.*, *27*, 4045–4048.

Anderson, B. J., H. Korth, C. L. Waters, D. L. Green, V. G. Merkin, R. J. Barnes, and L. P. Dyrud (2014), Development of large-scale Birkeland currents determined from the Active Magnetosphere and Planetary Electrodynamics Response Experiment, *Geophys. Res. Lett.*, *41*(9), 3017–3025, doi:10.1002/2014GL059941.

Birkeland, K. (1908), *The Norwegian Aurora Polaris Expedition 1902–1903*, vol. 1, H. Aschelhoug & Co., Christiania, Norway.

Birkeland, K. (1913), *The Norwegian Aurora Polaris Expedition 1902–1903*, vol. 2, H. Aschelhoug & Co., Christiania, Norway.

Clausen, L. B. N., J. B. H. Baker, J. M. Ruohoniemi, S. E. Milan, and B. J. Anderson (2012), Dynamics of the region 1 Birkeland current oval derived from the Active Magnetosphere and Planetary Electrodynamics Response Experiment (AMPERE), *J. Geophys. Res.*, *117*, A06233, doi:10.1029/2012JA017666.

Clausen, L. B. N., S. E. Milan, J. B. H. Baker, J. M. Ruohoniemi, K.-H. Glassmeier, J. C. Coxon, and B. J. Anderson (2013a), On the influence of open magnetic flux on substorm intensity: Ground- and space-based observations, *J. Geophys. Res. Space Physics*, *118*, 2958–2969, doi:10.1002/jgra.50308.

Clausen, L. B. N., J. B. H. Baker, J. M. Ruohoniemi, S. E. Milan, J. C. Coxon, S. Wing, S. Ohtani, and B. J. Anderson (2013b), Temporal and spatial dynamics of the regions 1 and 2 Birkeland currents during substorms, *J. Geophys. Res. Space Physics*, *118*, 3007–3016, doi:10.1002/jgra.50288.

Cohen, J., P. Cohen, S. G. West, and L. S. Aiken (2003), *Applied Multiple Regression/Correlation Analysis for the Behavioral Sciences*, 3rd ed., Lawrence Erlbaum Associates, Mahwah, N. J.

Cowley, S. W. H. (2000), Magnetosphere-ionosphere interactions: A tutorial review, in *Magnetospheric Current Systems, Geophys. Monogr. Ser.*, vol. 118, pp. 91–106, AGU, Washington, D. C.

Cowley, S. W. H., and M. Lockwood (1992), Excitation and decay of solar wind-driven flows in the magnetosphere-ionosphere system, *Ann. Geophys.*, *10*, 103–115.

Dungey, J. W. (1961), Interplanetary magnetic field and the auroral zones, *Phys. Rev. Lett.*, *6*, 47–48.

Gjerloev, J. W., S. Ohtani, T. Iijima, B. Anderson, J. Slavin, and G. Le (2011), Characteristics of the terrestrial field-aligned current system, *Ann. Geophys.*, *29*(10), 1713–1729, doi:10.5194/angeo-29-1713-2011.

Gonzalez, W. D., and F. S. Mozer (1974), A quantitative model for the potential resulting from reconnection with an arbitrary interplanetary magnetic field, *J. Geophys. Res.*, *79*(28), 4186–4194, doi:10.1029/JA079i028p04186.

Grocott, A., J. A. Wild, S. E. Milan, and T. K. Yeoman (2009), Superposed epoch analysis of the ionospheric convection evolution during substorms: Onset latitude dependence, *Ann. Geophys.*, *27*(2), 591–600, doi:10.5194/angeo-27-591-2009.

He, M., J. Vogt, H. Lühr, E. Sorbalo, A. Blagau, G. Le, and G. Lu (2012), A high-resolution model of field-aligned currents through empirical orthogonal functions analysis (MFACE), *Geophys. Res. Lett.*, *39*, L18105, doi:10.1029/2012GL053168.

Holzer, R. E., R. L. McPherron, and D. A. Hardy (1986), A quantitative empirical model of the magnetospheric flux transfer process, *J. Geophys. Res.*, *91*(A3), 3287–3293, doi:10.1029/JA091iA03p03287.

Iijima, T., and T. A. Potemra (1976a), The amplitude distribution of field-aligned currents at northern high latitudes observed by Triad, *J. Geophys. Res.*, *81*, 2165–2174.

Iijima, T., and T. A. Potemra (1976b), Field-aligned currents in the dayside cusp observed by Triad, *J. Geophys. Res.*, *81*, 5971–5979.

Iijima, T., and T. A. Potemra (1978), Large-scale characteristics of field-aligned currents associated with substorms, *J. Geophys. Res.*, *83*, 599–615.

Imber, S. M., S. E. Milan, and B. Hubert (2006), The auroral and ionospheric flow signatures of dual lobe reconnection, *Ann. Geophys.*, *24*(11), 3115–3129, doi:10.5194/angeo-24-3115-2006.

Juusola, L., S. E. Milan, M. Lester, A. Grocott, and S. M. Imber (2014), Interplanetary magnetic field control of the ionospheric field-aligned current and convection distributions, *J. Geophys. Res. Space Physics*, *119*, 3130–3149, doi:10.1002/2013JA019455.

Lockwood, M. (1991), On flow reversal boundaries and transpolar voltage in average models of high-latitude convection, *Planet. Space Sci.*, *39*(3), 397–409, doi:10.1016/0032-0633(91)90002-R.

Milan, S. E. (2013), Modeling Birkeland currents in the expanding/contracting polar cap paradigm, *J. Geophys. Res. Space Physics*, *118*(9), 5532–5542, doi:10.1002/jgra.50393.

Milan, S. E., M. Lester, S. W. H. Cowley, K. Oksavik, M. Brittnacher, R. A. Greenwald, G. Sofko, and J.-P. Villain (2003), Variations in the polar cap area during two substorm cycles, *Ann. Geophys.*, *21*(5), 1121–1140, doi:10.5194/angeo-21-1121-2003.

Milan, S. E., G. Provan, and B. Hubert (2007), Magnetic flux transport in the Dungey cycle: A survey of dayside and nightside reconnection rates, *J. Geophys. Res.*, *112*, A01209, doi:10.1029/2006JA011642.

Milan, S. E., J. S. Gosling, and B. Hubert (2012), Relationship between interplanetary parameters and the magnetopause reconnection rate quantified from observations of the expanding polar cap, *J. Geophys. Res.*, *117*, A03226, doi:10.1029/2011JA017082.

Neter, J., W. Wasserman, and G. A. Whitmore (1988), *Applied Statistics*, 3rd ed., Allyn and Bacon, Inc., Boston, Mass.

Newell, P. T., and J. W. Gjerloev (2011a), Evaluation of SuperMAG auroral electrojet indices as indicators of substorms and auroral power, *J. Geophys. Res.*, *116*, A12211, doi:10.1029/2011JA016779.

Newell, P. T., and J. W. Gjerloev (2011b), Substorm and magnetosphere characteristic scales inferred from the SuperMAG auroral electrojet indices, *J. Geophys. Res.*, *116*, A12232, doi:10.1029/2011JA016936.

Papitashvili, V. O. (2002), A new model of field-aligned currents derived from high-precision satellite magnetic field data, *Geophys. Res. Lett.*, *29*(14), 1683, doi:10.1029/2001GL014207.

Rostoker, G., M. Mareschal, and J. C. Samson (1982), Response of dayside net downward field-aligned current to changes in the interplanetary magnetic field and to substorm perturbations, *J. Geophys. Res.*, *87*(A5), 3489–3510, doi:10.1029/JA087iA05p03489.

Waters, C. L., B. J. Anderson, and K. Liou (2001), Estimation of global field-aligned currents using the Iridium® System magnetometer data, *Geophys. Res. Lett.*, *28*, 2165–2168.

Zmuda, A. J., J. H. Martin, and F. T. Heuring (1966), Transverse magnetic disturbances at 1100 kilometers in the auroral region, *J. Geophys. Res.*, *71*, 5033–5045.